2022 International Conference on Unmanned Aircraft Systems (ICUAS)
Dubrovnik, Croatia. June 21-24, 2022

Aerial Device Delivery for Power Line Inspection and Maintenance

Alejandro Suarez, Rafael Salmoral, Ambar Garofano-Soldado, Guillermo Heredia, and Anibal Ollero

2022 International Conference on Unmanned Aircraft Systems (ICUAS) | 978-1-6654-0593-5/22/$31.00 ©2022 IEEE | DOI: 10.1109/ICUAS54217.2022.9836039

***Abstract*— The inspection and maintenance of power lines with aerial robots requires to decrease as much as possible the performance time given the limited capacity of the batteries and the vast extension of this kind of infrastructure. In order to avoid the waste of time associated to the take-off and landing maneuvers, this paper proposes the use of aerial manipulation robots for fast and safe delivery in flight of devices and tools. Two use cases are considered. In the first one, a device delivery multirotor (DDM) is used as supplier for a device installation robot (DIR), consisting of a dual arm aerial manipulator in long reach configuration. The vertical separation distance between DIR and DDM associated to the long reach link contributes to reduce the risk of collision and the downwash effect over the DDM. In the second case, the DIR is used to deliver tools to human operators quickly and safely, avoiding hazardous situations during the handover thanks to the long reach configuration. The paper also analyzes the aerodynamic downwash effect of two multirotors flying vertically at distances determined by the long reach link through Computational Fluid Dynamics (CFD) simulation. Experimental results in an indoor testbed validate the proposed application.**

I. INTRODUCTION

The use of aerial robots for the inspection and maintenance of the power grid [1] aims to reduce the time and cost for the companies responsible of its management. The installation and removal of devices like bird flight diverters (helical and clip type), spacers and insulators are common tasks conducted nowadays by human operators working on the power lines or deployed through elevated lift platforms or manned helicopters. The high altitude (15 – 50 m) and high voltage (15 – 500 kV) of the power lines make these operations particularly risky, even more taking into account the vast extension of this infrastructure in any country, with tens of thousands of kilometers. These factors, along with the current achievements in the field, have motivated the interest in the development of aerial manipulation robots capable of performing these operations in a safe and reliable way [2], [3]. The ability of aerial manipulators to reach easily and quickly high altitude workspaces and interact with the environment has led to the rise of a number of applications like inspection in oil and gas refineries [4], [5], contact-based inspection of surfaces [6], or crack repair [7]. The functionalities and capabilities of aerial manipulators developed in the last years are described in [8], [9], [10]. A relevant aspect in these aerial manipulators is the coordinated control of the aerial platform and the arms [11].

A. Suarez (asuarezfm@us.es), R. Salmoral (rafaslasla@gmail.com), A. Garofano (agarofano@us.es), G. Heredia (guiller@us.es), and A. Ollero (aollero@us.es) are with the Institute of Robotics and Intelligent Systems (RIS-GRVC) of the University of Seville, Spain: https://grvc.us.es/

In some applications, several aerial robots have to operate in the same area. Multirotor aerial robots flying in close cooperation or in swarms may suffer from the aerodynamic interference of one of them entering the rotor downwash of the others [12]. This problem has been tackled in large teams of quadrotors planning trajectories that avoid entering the downwash of other robots [13]. Another solution adopted for airborne docking consists of separating several meters the docking point using a winch in order to decrease the downwash effect [14].

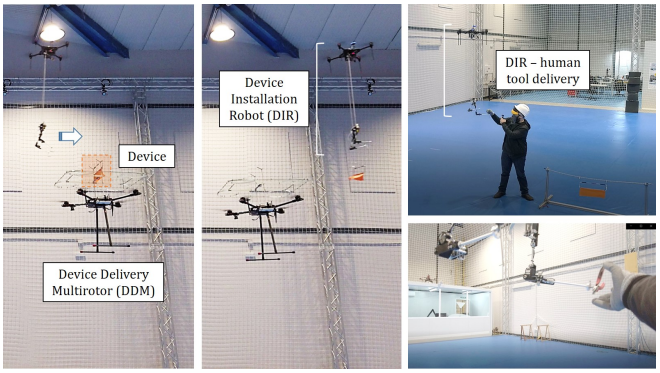

Fig. 1. Aerial device delivery between aerial robots (left) and between an aerial manipulator and a human operator (right).

Aerial manipulators in long reach configuration [2], [3] and cable suspended aerial manipulators [15], [16] result especially suitable when the proximity of environmental obstacles may compromise the safety of the robot, as is the case of the power lines, illustrated in Figure 1. Increasing the separation distance of the rotors and the manipulator also reduces the influence of the aerodynamic effects over the end effector or over other aerial vehicles flying below. This configuration[1] extends the effective workspace of the manipulator, typically constrained by the landing gear, allowing the realization of dexterous manipulation tasks like the installation of helical bird flight diverters in flight [1] or the safe interaction with human workers. The long reach link may also be useful for insulating electrically the aerial platform from the power line, protecting in this way the onboard components from the electromagnetic interference caused by the high voltage [3], [17], [18].

Despite the evident benefits of aerial manipulation robots, the reduced operation time (10 – 20 min) of multirotors due to the batteries is nowadays the main limitation in the

[1]In the following, we will employ indistinctly the terms long reach or cable suspended configurations, although this second term should not be confused with the power line.

practical application of this technology. In particular, the take-off and landing maneuvers, as well as the navigation phases, require a considerable time compared to the effective operation time [19]. In order to overcome this problem, some mechanisms have been developed for perching [20], [21].

The main contribution of this paper is the development and experimental validation of an aerial manipulation system for fast and safe delivery of devices and tools employed in the inspection and maintenance of power lines, as illustrated in Figure 1. Two use cases are considered. In the first one, a device delivery multirotor (DDM) carries the devices from the supply point to the device installation robot (DIR), conducting the operation in flight. The DIR is a cable suspended dual arm aerial manipulator, whereas the DDM is a multirotor with a support structure on top for carrying the device. The aerodynamic interaction between DIR and DDM during the device delivery phase will be studied in simulation through computational fluid dynamics (CFD) simulation. In the second case, the goal is to deliver hand tools to a human operator working on the power line, using for this purpose the DIR in long reach configuration to increase the separation distance between the operator's head and arms, and the propellers of the multirotor. The operator will be equipped with a helmet to obtain its relative position. Experimental results are presented in an indoor test-bed for validating both systems.

The rest of the paper is organized as follows. Section II introduces the intended application and describes both use cases. Section III describes the platforms and Section IV analyses in simulation the downwash effect. Experimental results are shown in Section V, presenting the conclusions in Section VI.

II. Application Description

A. Problem Formulation

Let us consider an illustrative scenario as the one depicted in Figure 2 consisting of three segments of power lines where it is necessary to install several devices as the ones considered in [1]. The installation points are marked as red circles and grouped in device installation areas. The devices are conveniently stored at a supply point (a van, for example) whose position is known. The installation points relative to the supply point, considered as the origin of the Earth fixed frame $\{\mathbf{E}\}$, are represented by $\mathbf{r}_j^i = [x_j^i, y_j^i, z_j^i]$, where i and j denote the installation area and particular point within that area, respectively. These points are supposed to be at constant height $z_j^i = h$ (15 m in this scenario). We assume that the first and last points of each area, that is, $\mathbf{r}_1^i$ and $\mathbf{r}_{N_i}^i$, correspond to the closest and furthest points with respect to the supply point, where N_i is the number of installation points in the i-th area.

Now, in order to improve the performance time in the installation of devices on the power lines, it is proposed the use of two aerial robots: 1) the DDM, which carries the device from the supply point to the proximity of the installation area, and 2) the DIR, who receives the device from the DDM (in flight) and conducts the installation

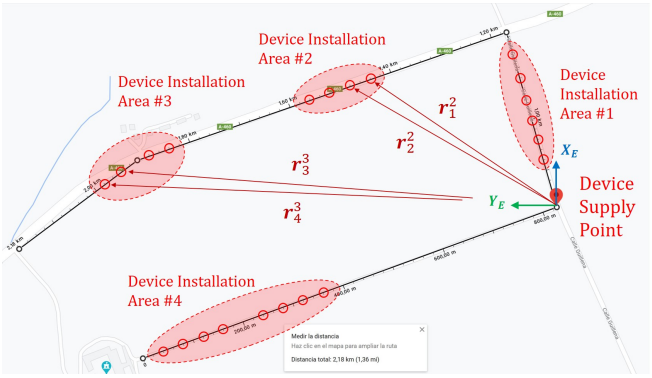

Fig. 2. Real scenario with power lines taken from Google maps illustrating four device installation areas with several installation points, 2.8 km length. The location of the supply point is determined by the traffic conditions.

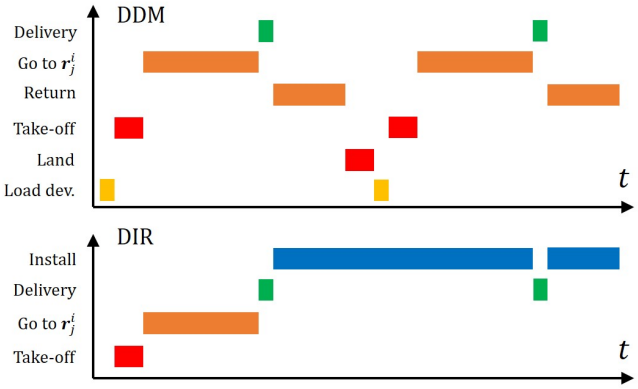

Fig. 3. Chronogram showing the operation of the DDM and the DIR for the delivery and installation of devices like the helical bird diverter.

operation. Taking into account that the time required to complete the installation of complex devices as helical bird diverters [1] may be significant, the idea here is to parallelize the delivery and installation phases, as depicted in Figure 3.

For convenience, and taking into account that the take-off and landing maneuvers in a multirotor are typically executed in the vertical axis, we introduce the horizontal position vector $\mathbf{p}_j^i = [x_j^i, y_j^i]$ to express the time required by the DDM to supply all the devices to the DIR as follows:

$$t_{DDM} = 2\sum_{i=1}^{N_a}\sum_{j=1}^{N_i}\left(\frac{\|\mathbf{p}_j^i\|}{v_{xy}^{DDM}} + \frac{z_j^i}{v_z^{DDM}} + \frac{t_D + t_L}{2}\right) \quad (1)$$

where N_a is the number of installation areas, $\|\cdot\|$ represents the Euclidean distance, v_{xy}^{DDM} and v_z^{DDM} are the nominal speeds of the DDM in the XY and Z axes, respectively, whereas t_D is the time required to complete the delivery operation in flight and t_L is the time needed to load the device on the DDM at the supply point. The improvement in the performance time of the proposed two-aerial robots system is evidenced in the computation of the time required by the DIR to perform the installation of the devices supplied by the DDM:

$$t_{DIR} = \sum_{i=1}^{N_a} \left(t_1^i + \sum_{j=2}^{N_i} \frac{\|\mathbf{p}_j^i - \mathbf{p}_{j-1}^i\|}{v_{xy}^{DIR}} + t_{N_i} + N_i(t_D + t_I) \right) \quad (2)$$

where t_1^i and t_{N_i} are travelling times of the first and last points in the i-th installation area:

$$t_1^i = \frac{\|\mathbf{p}_1^i\|}{v_{xy}^{DIR}} + \frac{z_1^i}{v_z^{DIR}} \quad ; \quad t_{N_i} = \frac{\|\mathbf{p}_{N_i}^i\|}{v_{xy}^{DIR}} + \frac{z_{N_i}^i}{v_z^{DIR}} \quad (3)$$

and t_I is the time required to install the device. It is assumed in Equation 2 that the DIR goes back to the supply point for changing the batteries once all the devices of an area have been installed. Note also that the DDM velocity should be adjusted according to the DIR installation time to avoid wait times, as in the timeline shown in Figure 3.

B. Fast and Safe Aerial Tool Delivery to Human Operators

Operators working on live power lines may lose their tools accidentally while they are hanging from the cables, which is a problem due to the difficult access to this kind of workspace, requiring climbing the transmission tower and installing the safety harnesses. In order to avoid the waste of time for the operators, it is proposed the use of aerial manipulators in long reach [2] or cable suspended [15], [16] configurations for fast and safe tool delivery, as illustrated in Figure 1 and Figure 4. Increasing the separation distance between the manipulator and the propellers of the multirotor contributes to increase the comfort and safety perception of the operator, reducing also the risk of collision with the operator or with the power line, taking into account the presence of wind gusts in this kind of environments. It is desirable that both the manipulator and the aerial platform are as light as possible to reduce the potential damage in case of collision. The use of lightweight and compliant dual arms [2], [3] results in more intuitive human-robot interactions [22] and extends the load capacity of the manipulator, allowing for example the simultaneous transportation of two tools or of long objects.

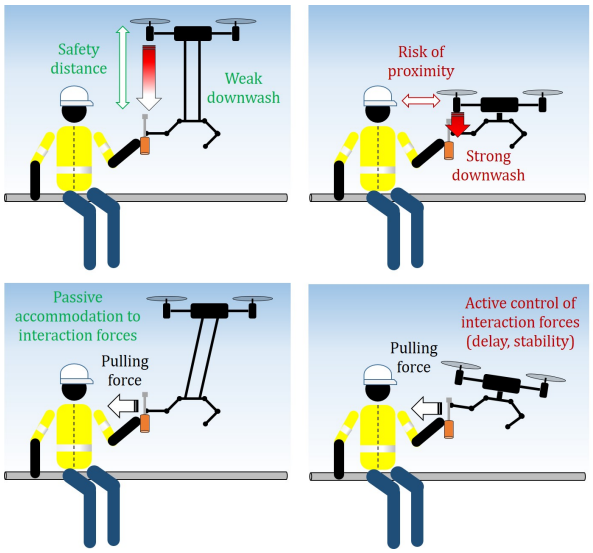

Fig. 4. Benefits of the aerial manipulator in long reach configuration (left) compared to the standard one (right) for aerial tool delivery to worker.

III. System Description

A. DDM and DIR

The multirotor platforms employed in the realization of the experiments are shown in Figure 5, indicating in Table I their main features. The first one is the Proskytec LM (Light Multirotor) quadrotor to be used for the fast delivery of tools to the human operator (Section V-A) and as DIR in the aerial device delivery test (Section V-C). The identification of the downwash effect raised when both platforms are flying on the same vertical axis will be carried out with two of these platforms (see Section V-B). In order to overcome the loss of thrust caused by this effect, a bigger quadrotor, the Proskytec LRM, is needed as DDM for the device delivery experiment. Note that the aerial platform employed for aerial coworking with the human operator should be as light as possible to reduce the risk and potential damage on the person, and should integrate the arms in cable suspended configuration to improve safety by increasing the separation distance between the human and the propellers. Both platforms employ a CUAV v5 autopilot, running Arducopter 3.6.1 and the UAL (UAV Abstraction Layer) [23] on a Rasbperry Pi model 3B+ to interface the autopilot and the OptiTrack positioning system. The LRM platform is equipped with a lightweight safety structure built in aluminum and PVC (polyvinyl chloride) profiles that support a light nylon mesh intended to prevent the impact of the device with the propellers in case the grasping maneuver fails. The device to be delivered in flight consists of an orange color band and a hook-like wire frame structure that facilitates the grasping and installation on the power line, as depicted in Figure 5.

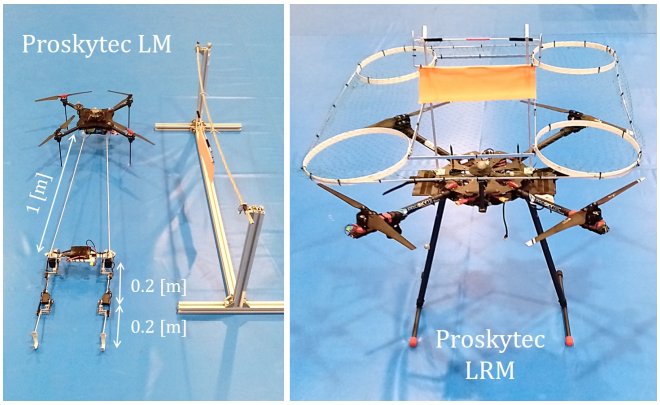

Fig. 5. Device Installation Robot equipped with dual arm manipulator in cable suspended configuration (left) and Device Delivery Multirotor equipped with safety net and device to be delivered (right).

B. Dual Arm Design

The grasping of the color marker on the power line, as well as the tool delivery to the human operator will be carried

TABLE I

MAIN FEATURES OF THE DIR AND DDM MULTIROTORS.

	Proskytec LRM	Proskytec LM
Weight [kg]	6	2
MTOW [kg]	9.5	3.5
Max. flight time [min]	45	50
Propellers [inch]	21 × 7	15 × 5.5
Wheelbase [mm]	1000	610
Central plate area [m^2]	0.06	0.05
Max asc. speed [m/s]	1.5	1.5
Max cruise speed [m/s]	3	3

out by the DIR with a lightweight and compliant dual arm system [3] shown in Figure 6, integrated in cable suspended configuration. Each of the arms provides two degrees of freedom in the usual upper arm (200 mm) forearm (200 mm) configuration, with 250 mm separation between them. The frame structure is manufactured in carbon fiber and aluminum, using the Herkulex DRS-0201 actuators in all the joints, integrating a compact spring-lever transmission mechanism (5 Nm/rad) to provide mechanical joint compliance. This will protect the actuators against the impact exerted when the device is grasped, resulting also in a more comfortable interaction for the human worker during the tool delivery operation. The shoulder structure of the arms supports the 2S 1800 mAh LiPo battery that feeds the dual arm, the Raspberry Pi Model 3B+ where the control program of the arms is executed and interfaced through a wireless SSH session from the ground control station, and a 5 V battery that feeds the computer board.

The arms are suspended from the multirotor base by two 1000 mm length cables. This solution was adopted instead of the double long reach aluminum link [2] since preliminary flight tests showed that, for this length, the multirotor position controller is laterally destabilized due to the high inertia of the attached load. However, and as evidenced in the video attachment, the manipulator does not oscillate significantly despite the free motion of the cables. This configuration provides four main benefits in this application:

1) Improve safety by increasing the separation between the propellers and the power line or the operator.
2) Reduce the downwash effect by increasing the distance between the DIR and the DDM.
3) Allows electrical insulation of the aerial platform to prevent the electrostatic discharge causing a fault [3].
4) Facilitates the landing once the arms lay on the ground.

In order to reduce the risk of entrapment in the realization of the delivery task, the end effector of the arms consists of a C-shaped frame used as hook-like gripper, employing magnets for the tool delivery task to the human operator.

IV. CFD ANALYSIS

A. Problem Formulation

This section presents the numerical simulations performed to analyse the static aerodynamic interaction of two multirotors (DIR and DDM) when hovering one over the other. The

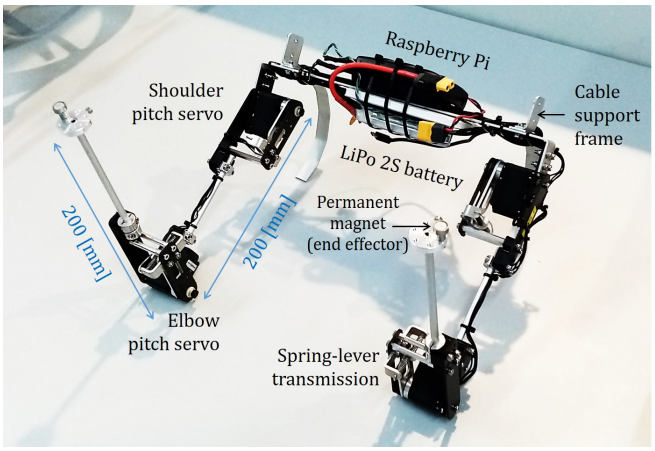

Fig. 6. Lightweight and compliant dual arm used to provide hand tools to the human operators, and retrieve the delivered devices.

velocity induced at the downstream flow of a multirotor leads to a decrease in the performance of another platform that step into such downwash. To obtain a preliminary estimation of the flow field characteristics and the interference of the DIR downwash on the DDM, a CFD (Computational Fluid Dynamics) analysis is carried out using ANSYS-FLUENT. The Incompressible Reynolds-Averaged Navier-Stokes equations (RANS) and the SST (shear stress transport) k-ω turbulence model are used in all simulations [24]. For this purpose, a second order numerical scheme is used for the convective and diffusive terms. The Navier-Stokes equations for an incompressible flow can be written as:

$$\nabla \cdot \mathbf{v} = 0 \tag{4}$$

$$\rho \frac{\partial \mathbf{v}}{\partial t} + \rho(\mathbf{v} \cdot \nabla)\mathbf{v} = -\nabla p + \mu \nabla^2 \mathbf{v} + \rho \mathbf{g} \tag{5}$$

where ρ is the air density, p is the static pressure, $\mathbf{v}$ is the flow velocity and $\rho\mathbf{g}$ are the gravitational body forces. In addition, the pressure-based steady solver is chosen. A coupled algorithm was selected to solve the problem as it allowed a faster convergence of the simulation.

The Multiple Reference Frame (MRF) method is applied to solve the aerodynamic flow in multiple zones. It is a steady-state approximation that provides accurate enough results with short computational time. Since we are interested in knowing the steady-state flow field and the change of thrust experienced by the rotors in static conditions, the MRF approach is considered [25], [26], [27], [28]. The MRF method divides the computational domain into two zones: eight rotating domains where a flow is induced with a constant angular speed, and a stationary domain. The following rotational speeds are considered for the two platforms shown in Figure 5:

- Proskytec LM multirotor: 15' × 5' T-Motor propeller at 4.500 RPM.
- Proskytec LRM multirotor: 21' × 6.3' T-Motor propeller at 3.500 RPM.

To obtain the angular speed of the rotors, two experimental

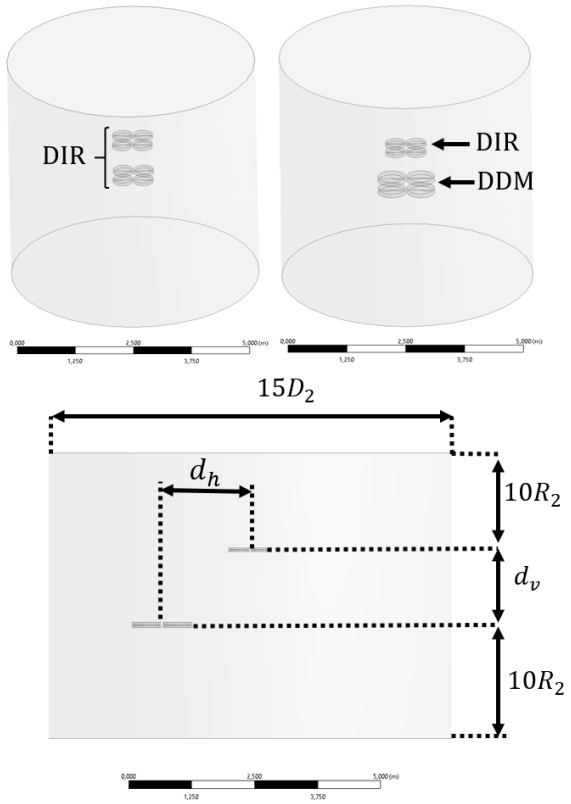

Fig. 7. Dimensions of the computational domain defined for different vertical (d_v) and horizontal distances (d_h).

tests have been carried out considering the payload of the robotic arm used in the experiments presented in Section V. Figure 7 shows the dimensions of the defined computational domain, where R_2 is the radius of the larger propeller. The central frame of the aerial platforms has not been considered because it has a negligible effect on the total thrust. The boundary conditions at the top and at the bottom of the stationary domain are pressure inlet and pressure outlet, respectively. In addition, some interfaces are created to separate the stationary domain from the rotational domain. Unstructured tetrahedral meshes are generated in this study. The convergence criterion was established when the values of the residuals reached 10^{-6} and the variables of interest did not change more than 0.1% in the last 1000 iterations.

In this study, two quadcopters separated vertically at a distance d_v of 1, 1.5 and 2 m and horizontally at a distance d_h of 0 and 1.5 m are considered. In addition, two different cases will be analysed: one case where the two multirotors will have the same dimensions and the other where they will be of different sizes, according to the platforms shown in Figure 5 employed in Section V-C. In the first case, eight T-Motor propellers with a diameter of 15 inches and a pitch of 5 inches is considered. For the second case, four 15' $\times$ 5' T-Motor propellers will be employed on the DIR and four T-Motor propellers with a diameter of 21 inches and a pitch of 6.3 inches will be used in the DDM.

TABLE II

THRUST COEFFICIENTS OBTAINED BY TWO AERIAL PLATFORMS VERTICALLY SEPARATED AT DIFFERENT DISTANCES (d_v) AND $d_h = 0$. THE UPPER MULTIROTOR HAVE 15'×5' T-MOTOR PROPELLERS AND THE LOWER MULTIROTOR HAVE 21' × 6.3' T-MOTOR PROPELLERS.

Distances d_v	C_t of UAV up	C_t of UAV down	C_t variation (%)
1	0.0333	0.0284	16.94
1.5	0.0334	0.0286	16.21
2	0.0334	0.0289	15.37

TABLE III

THRUST COEFFICIENTS OBTAINED BY TWO AERIAL PLATFORMS VERTICALLY SEPARATED AT DIFFERENT DISTANCES (d_v) AND $d_h = 0$. BOTH MULTIROTORS HAVE 15'×5' T-MOTOR PROPELLERS.

Distances d_v	C_t of UAV up	C_t of UAV down	C_t variation (%)
1	0.0335	0.0203	40.05
1.5	0.0335	0.0230	31.87
2	0.0335	0.0248	26.73

B. Simulation Results

This section shows the results obtained in the simulations described above. Table II and III show the total thrust coefficient obtained for both multirotor platforms. The thrust coefficient can be defined as follow:

$$C_t = \frac{T}{\rho A \Omega^2 R^2} \tag{6}$$

where T is the total thrust of the four propellers, ρ is the air density ($\rho = 1.225\ \frac{kg}{m^3}$), A is the area of the rotor disk, Ω is the rotational speed and R is the propeller radius. Specifically, Table II shows the results for the case in which both platforms have different dimensions and Table III for the case in which they are of the same sizes. In addition, both tables provide the percentage decrease of the thrust coefficient experienced by the lower UAV compared to the case where there is no interaction. As it can be seen, while the upper UAV remains at a constant thrust coefficient level, the lower UAV thrust coefficient decreases as the separation is reduced. This behaviour is observed in the results shown in Section V-C. When the downstream flow from the upper aerial platform interacts with the bottom platform, the lower platform experiences a decrease in thrust. In this case, the rotational speed of the lower UAV has to be increased to maintain its hover position and the vertical separation with the other platform. Moreover, the downwash effect becomes more noticeable when both platforms have the same dimensions. This is because the area affected by the flow on the lower UAV is completely covered when positioned directly above it. Also, the airflow from the upper propellers reduces the effective thrust of the lower propellers.

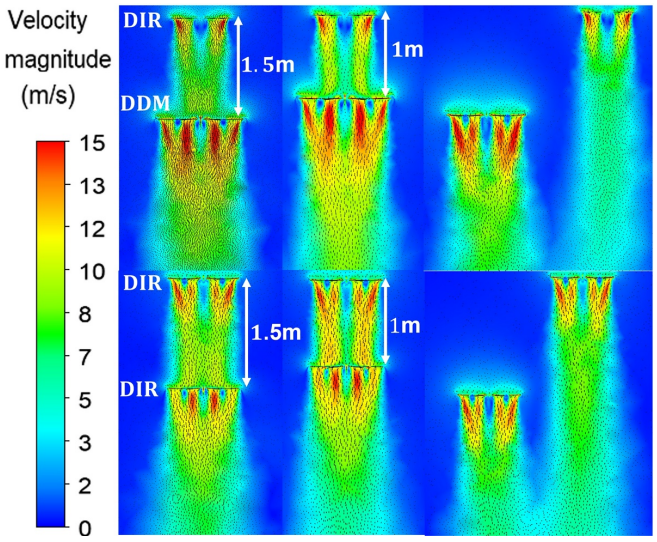

Fig. 8. Velocity and vector field contour for both the case of UAVs with the same (15 × 5 inch T-Motor propeller) and different (21 × 6.3 inch T-Motor propeller) dimensions for vertical distances of 1 and 1.5 m and horizontal distances of 0 and 1.5 m.

Figure 8 shows the velocity contour and vector field for the case in which both aerial platforms have the same dimensions (bottom images) and different dimensions (top images). The behaviour of the flow field is represented for the case d_v is 1 and 1.5 m, and d_h is 0 and 1.5 m. It can be observed that, when both multirotors have the same dimensions, the velocity field is higher as the flow of each propeller above impacts with each lower propeller. This analysis provides an approximation of the flow behaviour in critical situations when an aerial platform has to operate in close proximity to other platforms to perform a specific task.

V. Experimental Results

This section presents experimental results that validate the use of the DDM for aerial delivery of tools to a human operator, and devices to be installed on a power line to the DIR. The aerodynamic downwash effect between the multirotors is also experimentally identified to determine which is the best approach to conduct the delivery operation attending to the perturbation on the position controller. The video of the experiments can be found in [29].

A. Aerial Tool Delivery to Human Operator

The goal of this experiment is to illustrate the application of the dual arm aerial manipulator in long reach configuration for fast and safe tool delivery to human operators working on the power lines. The task consists of providing a screwdriver and some pliers to an operator by using the DIR described in Section III. Figure 9 shows the sequence of images from the video. The operator is equipped with safety goggles, face shield, gloves, and a safety helmet with Opti-Track markers used to measure the position of the aerial robot relative to the operator's head, depicted in Figure 10. Visual markers or ultra-violet LEDs [30] could be employed in real outdoor conditions replacing the indoor localization system. The end effector of the robotic arms, tele-operated from the ground control station, employs two magnets to facilitate the grasping of the objects, avoiding the risk of entrapment. The aerial platform is controlled in position mode, determining empirically the relative position between the robot and the operator based on his/her feeling of safety and comfort.

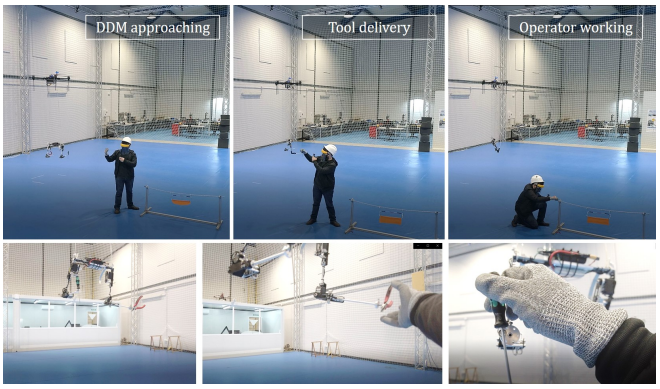

Fig. 9. Sequence of images showing the aerial tool delivery to a human operator working on the power line.

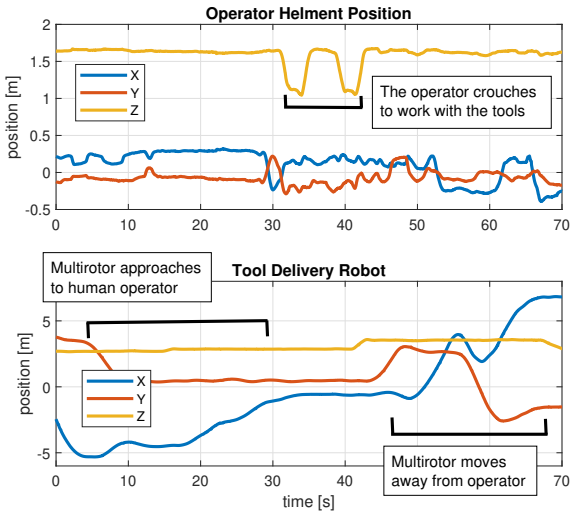

Fig. 10. Position of human worker's helmet and multirotor platform during the aerial tool delivery operation.

B. Evaluation of the Downwash Effect on the DDM

The purpose of this experiment is three fold: 1) compare qualitatively the behavior of the DIR and DDM multirotors with the CFD results presented in Section IV, estimating the increment in the thrust of the DDM for different distances when the DIR is flying above; 2) determine the most convenient approaching strategy (vertical or lateral) between DDM and DIR as previous step to conduct the aerial device delivery; 3) evaluate the performance of the Ardupilot controller implemented in the Pixhawk of the DDM when this is controlled in position and affected by the downwash generated by the DIR. In this experiment, two identical

Proskytec LM platforms as the ones described in Section III-A will be used as DIR and DDM, removing the dual arm from the DIR. Both platforms are controlled in position mode using an Opti-Track system. The DDM will hover at $z_{DDM}^{ref} = 3$ m. At this height the ground effect is negligible. Two approaching maneuvers are considered for the DIR platform. In the vertical approach, the DIR approaches from above with an initial height $z_{DIR}^{ref} = 5$ m. Once the DIR is at the same XY position as the DDM, it decreases its height slowly until the vertical distance d between them is 1 m. Figure 11 represents the evolution of the attitude of both platforms during the experiment, identifying the moment when the downwash produced by the DIR causes an attitude-position disturbance on the DDM controller between t = 180 and t = 280 s. The variation in thrust of the two platforms in the same interval is depicted in Figure 12.

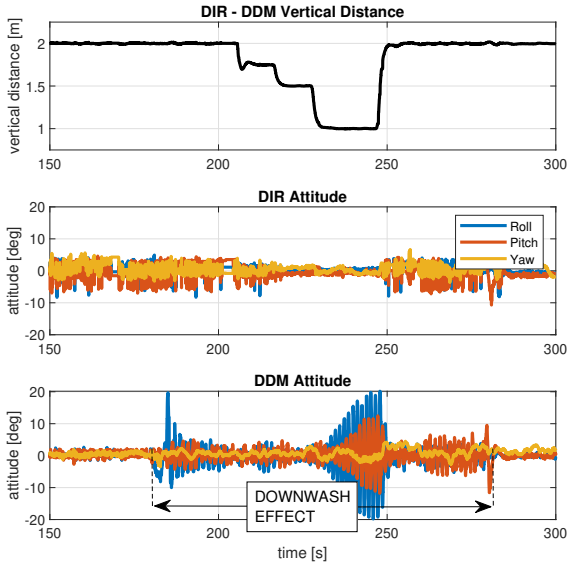

Fig. 11. Attitude of DIR (middle) and DDM (down) for different vertical separation distances (up). The DDM hovers at fixed position at $[XYZ] = [0, 0, 3]$ m while the DIR approaches vertically from $z = 5$ to $z = 4$ m.

C. Aerial Device Delivery

In this experiment, the DIR is equipped with the dual arm system described in Section III-B in cable suspended configuration, using as DDM the platform with the safety structure shown in Figure 5 to avoid that the device to be delivered impacts the propellers in case the capture fails. The end effector of the arms is a C-shaped aluminum frame (hook) that facilitates the grasping. In the experiment, the device to be installed is held by a frame structure at the top of the DDM, which is hovering in a position close the power line. Then, the DIR performs the passing approach to grasp the device flying 2.15 m above the DDM, with the arms partially stretched to increase the separation distance. Figure 13 illustrates the sequence of images taken from the video, whereas Figure 14 represents the trajectory of both platforms during the approaching and capture maneuvers. As it can be

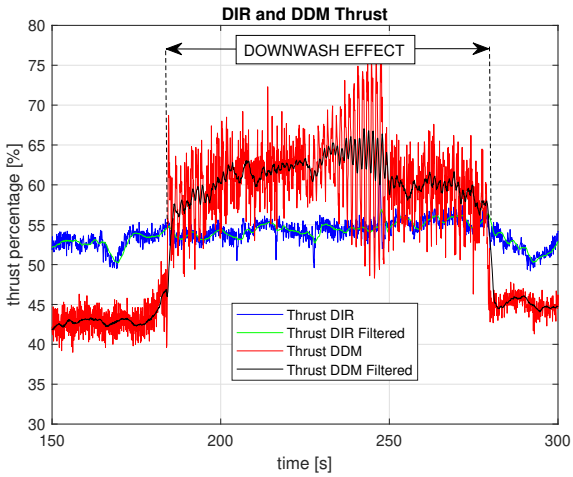

Fig. 12. Rotors thrust (in %) of DDM and DIR platforms for different vertical separation distances. The downwash effect occurs at t = 180 s when the DDM enters in the area of the DIR.

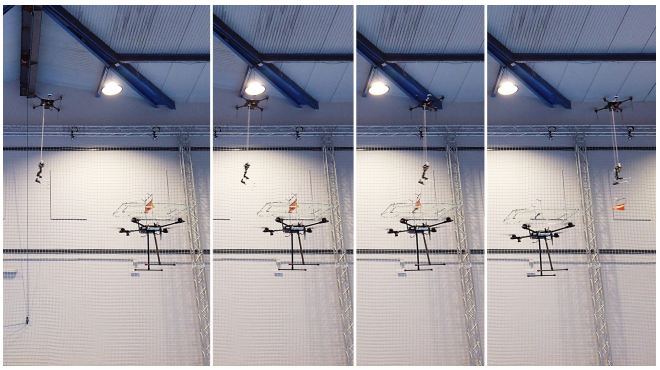

Fig. 13. Sequence of images representing the aerial device delivery with the pass-approach. The DDM hovers at fixed position while the DIR flies to grasp the device.

seen, there is a certain perturbation in the attitude and a position deviation in the DDM when the arms of the DIR catch the device around t = 56.5 s.

VI. CONCLUSIONS

This paper presented an aerial delivery system consisting of a device installer robot and a device delivery multirotor, intended to improve the performance time in the maintenance of power lines. Experimental results evidenced the influence of the DIR over the DDM position controller when both are flying closely with the same vertical axis due to the downwash effect, analyzed through CFD simulation. The paper showed the feasibility to perform fast and safe tool delivery to human operators, and the most suited approach for grasping in flight the device. As future work, it is proposed the evaluation of the tilted rotor and other configurations to reduce the effect of this perturbation.

ACKNOWLEDGMENT

This work is supported by the AERIAL-CORE project (H2020-2019-871479) funded by the European Commission, the ROBMIND project (PDC2021-121524-I00) funded by

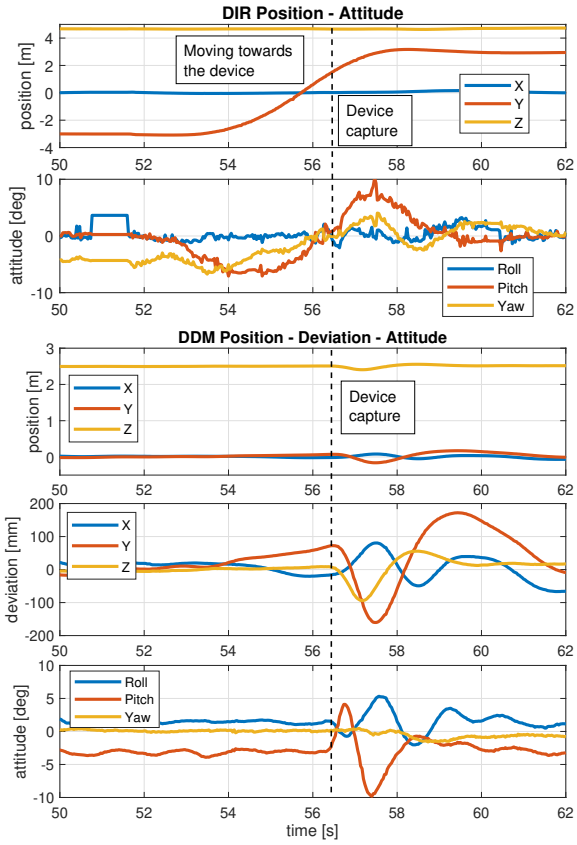

Fig. 14. Evolution of DIR and DDM platforms during the approaching and device capture phases.

the Spanish Ministerio de Ciencia e Innovacion, and the ARTIC project (RTI2018-102224-B-I00), funded by the Spanish Ministerio de Economia, Industria, y Competitividad.

The work of Alejandro Suarez is funded by the Consejería de Transformación Económica, Industria, Conocimiento y Universidades de la Junta de Andalucía (Spain) through a post-doctoral research grant. The work of Ambar Garofano-Soldado is supported by the FPI grant from the Ministry of Science and Innovation of the Spanish Government.

Authors want to thank the contribution of Manuel Fernandez in the realization of the flight experiments, particularly in the aerial tool delivery in which he played the role of power line operator.

REFERENCES

[1] J. Cacace, S. M. Orozco-Soto, A. Suarez, A. Caballero, M. Orsag, S. Bogdan, G. Vasiljevic, E. Ebeid, J. A. A. Rodriguez, and A. Ollero, "Safe local aerial manipulation for the installation of devices on power lines: Aerial-core first year results and designs," *Applied Sciences*, vol. 11, no. 13, 2021. [Online]. Available: https://www.mdpi.com/2076-3417/11/13/6220

[2] A. Suarez, F. Real, V. M. Vega, G. Heredia, A. Rodriguez-Castano, and A. Ollero, "Compliant bimanual aerial manipulation: Standard and long reach configurations," *IEEE Access*, vol. 8, pp. 88 844–88 865, 2020.

[3] A. Suarez, R. Salmoral, P. J. Zarco-Periñan, and A. Ollero, "Experimental evaluation of aerial manipulation robot in contact with 15 kv power line: Shielded and long reach configurations," *IEEE Access*, vol. 9, pp. 94 573–94 585, 2021.

[4] M. Á. Trujillo, J. R. Martínez-de Dios, C. Martín, A. Viguria, and A. Ollero, "Novel aerial manipulator for accurate and robust industrial ndt contact inspection: A new tool for the oil and gas inspection industry," *Sensors*, vol. 19, no. 6, p. 1305, 2019.

[5] M. Tognon, H. A. T. Chávez, E. Gasparin, Q. Sablé, D. Bicego, A. Mallet, M. Lany, G. Santi, B. Revaz, J. Cortés *et al.*, "A truly-redundant aerial manipulator system with application to push-and-slide inspection in industrial plants," *IEEE Robotics and Automation Letters*, vol. 4, no. 2, pp. 1846–1851, 2019.

[6] K. Bodie, M. Brunner, M. Pantic, S. Walser, P. Pfändler, U. Angst, R. Siegwart, and J. Nieto, "Active interaction force control for contact-based inspection with a fully actuated aerial vehicle," *IEEE Transactions on Robotics*, vol. 37, no. 3, pp. 709–722, 2020.

[7] P. Chermprayong, K. Zhang, F. Xiao, and M. Kovac, "An integrated delta manipulator for aerial repair: A new aerial robotic system," *IEEE Robotics & Automation Magazine*, vol. 26, no. 1, pp. 54–66, 2019.

[8] A. Ollero, M. Tognon, A. Suarez, D. Lee, and A. Franchi, "Past, present, and future of aerial robotic manipulators," *IEEE Transactions on Robotics*, vol. 38, no. 1, pp. 626–645, 2022.

[9] M. Orsag, C. Korpela, P. Oh, S. Bogdan, and A. Ollero, *Aerial manipulation*. Springer, 2018.

[10] X. Meng, Y. He, and J. Han, "Survey on aerial manipulator: System, modeling, and control," *Robotica*, vol. 38, no. 7, pp. 1288–1317, 2020.

[11] K. Baizid, G. Giglio, F. Pierri, M. A. Trujillo, G. Antonelli, F. Caccavale, A. Viguria, S. Chiaverini, and A. Ollero, "Behavioral control of unmanned aerial vehicle manipulator systems," *Autonomous Robots*, vol. 41, no. 5, pp. 1203–1220, 2017.

[12] K. P. Jain, T. Fortmuller, J. Byun, S. A. Mäkiharju, and M. W. Mueller, "Modeling of aerodynamic disturbances for proximity flight of multirotors," in *2019 International Conference on Unmanned Aircraft Systems (ICUAS)*. IEEE, 2019, pp. 1261–1269.

[13] J. A. Preiss, W. Hönig, N. Ayanian, and G. S. Sukhatme, "Downwash-aware trajectory planning for large quadrotor teams," in *2017 IEEE/RSJ International Conference on Intelligent Robots and Systems (IROS)*. IEEE, 2017, pp. 250–257.

[14] R. Miyazaki, R. Jiang, H. Paul, K. Ono, and K. Shimonomura, "Aerial docking for multi-rotor aerial manipulations," in *2018 IEEE/RSJ International Conference on Intelligent Robots and Systems (IROS)*. IEEE, 2018, pp. 4708–4714.

[15] Y. S. Sarkisov, M. J. Kim, D. Bicego, D. Tsetserukou, C. Ott, A. Franchi, and K. Kondak, "Development of sam: cable-suspended aerial manipulator," in *2019 International Conference on Robotics and Automation (ICRA)*. IEEE, 2019, pp. 5323–5329.

[16] R. Miyazaki, H. Paul, T. Kominami, and K. Shimonomura, "Wire-suspended device control based on wireless communication with multirotor for long reach-aerial manipulation," *IEEE Access*, vol. 8, pp. 172 096–172 104, 2020.

[17] M. Heggo, K. Kabbabe, V. Peesapati, R. Gardner, S. Watson, and W. Crowther, "Operation of aerial inspections vehicles in hvdc environments part a: Evaluation and mitigation of high electrostatic field impact," in *Journal of Physics: Conference Series*, vol. 1356, no. 1. IOP Publishing, 2019, p. 012009.

[18] D. Yu, S. Wan, F. Chen, X. Bian, L. Chen, M. MacAlpine, J. Zhang, L. Zhang, and L. Wang, "The effect of floating-potential conductors on the electric field near overhead transmission lines," *Journal of Electrostatics*, vol. 70, no. 3, pp. 339–345, 2012.

[19] A. Suarez, V. M. Vega, M. Fernandez, G. Heredia, and A. Ollero, "Benchmarks for aerial manipulation," *IEEE Robotics and Automation Letters*, vol. 5, no. 2, pp. 2650–2657, 2020.

[20] H. W. Wopereis, T. Van Der Molen, T. Post, S. Stramigioli, and M. Fumagalli, "Mechanism for perching on smooth surfaces using aerial impacts," in *2016 IEEE international symposium on safety, security, and rescue robotics (SSRR)*. IEEE, 2016, pp. 154–159.

[21] C. E. Doyle, J. J. Bird, T. A. Isom, J. C. Kallman, D. F. Bareiss, D. J. Dunlop, R. J. King, J. J. Abbott, and M. A. Minor, "An avian-inspired passive mechanism for quadrotor perching," *IEEE/ASME Transactions On Mechatronics*, vol. 18, no. 2, pp. 506–517, 2012.

[22] A. Gómez Eguíluz, I. Rañó, S. A. Coleman, and T. M. McGinnity, "Reliable robotic handovers through tactile sensing," *Autonomous Robots*, vol. 43, no. 7, pp. 1623–1637, 2019.

[23] F. Real, A. Torres-Gonzalez, P. Ramón-Soria, J. Capitán, and A. Ollero, "Ual: An abstraction layer for unmanned aerial vehicles," in *2nd International Symposium on Aerial Robotics*, 2018.

[24] E. Loureiro, N. Oliveira, P. Hallak, F. Bastos, L. Rocha, R. Delmonte, and A. Lemonge, "Evaluation of low fidelity and cfd methods for the

aerodynamic performance of a small propeller," *Aerospace Science and Technology*, vol. 108, p. 106402, 01 2021.
[25] X. Wang, Y. Liu, and C. Huang, "Research on finite ground effect of a rotor," pp. 6935–6940, 2019.
[26] A. Garofano-Soldado, G. Heredia, and A. Ollero, "Aerodynamic interference in confined environments with tilted propellers: Wall effect and corner effect," in *2021 Aerial Robotic Systems Physically Interacting with the Environment (AIRPHARO)*, 2021, pp. 1–8.
[27] C. Paz, E. Suarez, C. Gil, and C. Baker, "Cfd analysis of the aerodynamic effects on the stability of the flight of a quadcopter uav in the proximity of walls and ground," *Journal of Wind Engineering and Industrial Aerodynamics*, vol. 206, p. 104378, 2020.
[28] P. A. Silva, P. Tsoutsanis, and A. F. Antoniadis, "Simple multiple reference frame for high-order solution of hovering rotors with and without ground effect," *Aerospace Science and Technology*, vol. 111, p. 106518, 2021.
[29] "Experiments:," https://www.youtube.com/watch?v=j00RQOhKANg, accessed: 2022-02-18.
[30] V. Walter, N. Staub, A. Franchi, and M. Saska, "Uvdar system for visual relative localization with application to leader–follower formations of multirotor uavs," *IEEE Robotics and Automation Letters*, vol. 4, no. 3, pp. 2637–2644, 2019.